Exact pretransition effects in kinetically constrained circuits: Dynamical fluctuations in the Floquet-East model

Katja Klobas [ORCID], Cecilia De Fazio [ORCID], and Juan P. Garrahan [ORCID]

School of Physics and Astronomy, University of Nottingham, Nottingham NG7 2RD, United Kingdom
and Centre for the Mathematics and Theoretical Physics of Quantum Non-Equilibrium Systems,
University of Nottingham, Nottingham NG7 2RD, United Kingdom

We study the dynamics of a classical circuit corresponding to a discrete-time version of the kinetically constrained East model. We show that this classical "Floquet-East" model displays pre-transition behavior which is a dynamical equivalent of the hydrophobic effect in water. For the deterministic version of the model, we prove exactly (i) a change in scaling with size in the probability of inactive space-time regions (akin to the "energy-entropy" crossover of the solvation free energy in water), (ii) a first-order phase transition in the dynamical large deviations, (iii) the existence of the optimal geometry for local phase separation to accommodate space-time solutes, and (iv) a dynamical analog of "hydrophobic collapse."

Introduction. In thermodynamics, proximity to a phase transition gives rise to pretransition effects in the presence of surfaces or solutes. For systems near criticality this leads to the Casimir effect [1–4]. The equivalent for first-order transitions is the hydrophobic effect as occurs in water [5–8]: near liquid-vapor coexistence, the free-energy to accommodate a solute [7,8] displays an entropic-energetic crossover, from scaling with volume for small solutes to scaling with area for larger ones, since it becomes favorable to create a vapor domain around the solute paying only an interface cost (see also [5,6]). Hydrophobicity generalizes to other systems with first-order transitions, known as the "orderphobic effect" [9].

Hydrophobiclike physics appears, at least numerically [10], to also manifest in the dynamical fluctuations of kinetically constrained models (KCMs) [11–13]. These are models with explicit constraints in the dynamics that help explain [14–16] many features relating to the glass transition [17,18]. Specifically, in terms of KCMs [19] dynamic heterogeneity can be understood as mesoscopic space-time fluctuations related to a nearby active/inactive first-order transition in the space of trajectories [20–22] found via dynamical large deviation methods [23–25] (cf. full-counting statistics [26]). Beyond the glass problem, constrained dynamics is of interest in several other areas. These include cellular automata (CA) [27–29], whose dynamics can also be understood in terms of local constraints; quantum many-body systems such as driven Rydberg atoms which can behave like KCMs [30–33]; slow quantum thermalization [34–39]; quantum scars [40,41]; and fractonic systems [42,43].

In this paper we prove dynamical hydrophobicity (i.e., pretransition effects) analytically beyond just numerics [10] for deterministic KCMs. We do so by studying a classical system with discrete-space/discrete-time "circuit" dynamics with the same local constraint as the (continuous-time) stochastic East model [12,13]. For the deterministic version of this "Floquet-East" model—where the circuit gates are unitary (i.e., permutations)—we demonstrate by means of exact calculations all the relevant features of hydrophobicity in the dynamics: a crossover in the scaling of the probability of inactive space-time regions, a first-order phase transition in the dynamical large deviations, an optimal geometry to accommodate space-time solutes, and the dynamical analog of "hydrophobic collapse." Furthermore, the relevance of the deterministic results is that they bound properties of the dynamics in the presence of stochastic gates with the same constraint, which allows to prove dynamical hydrophobicity exactly also in the stochastic Floquet East model [44]. Below, we present our main results while the Supplemental Material (SM) [45] contains additional proofs and details of calculations.

Floquet-East model. We consider a chain of $2L$ sites with a binary variable (or classical spin) per site $n_i \in \{0, 1\}$, with the site labels i taking half-integer values, $i \in \{\frac{1}{2}, 1, \frac{3}{2}, \ldots, L\}$. Relevant statistical states are probability vectors $|P\rangle := \sum_n |n\rangle P(n)$, where $\{|n\rangle := |n_{\frac{1}{2}}\rangle \otimes |n_1\rangle \otimes \cdots \otimes |n_L\rangle\}$ is the configurational basis, $P(n) \geqslant 0 \; \forall n$, and $\langle - | P = \sum_n P(n) = 1$ (with $\langle - | := \sum_n \langle n|$ the "flat state"). The dynamics is discrete, staggered in terms of two half time-steps given by the deterministic maps U^{e} and U^{o},

$$|P_{t+1}\rangle = U^{\mathrm{e}} |P_{t+\frac{1}{2}}\rangle = U^{\mathrm{e}} U^{\mathrm{o}} |P_t\rangle, \quad t \in \mathbb{N}. \qquad (1)$$

The maps U^{e} and U^{o} consist of two-site gates u applied either to even or odd pairs of neighboring sites,

$$U^{\mathrm{e}} = u^{\otimes L}, \quad U^{\mathrm{o}} = \Pi_L u^{\otimes L} \Pi_L^{\dagger}, \qquad (2)$$
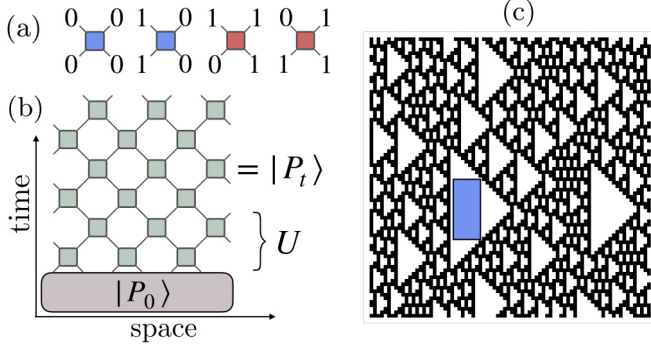
FIG. 1. Floquet-East model. (a) Allowed local gates: the left spin can flip only if its right neighbor is one; spin-flip gates are shaded red, no-flip gates shaded blue. (b) Tensor-network representation of an initial state $|P_0\rangle$ evolved under the Floquet dynamics, $|P_t\rangle = U^t |P_0\rangle$. (c) Sample trajectory from a random initial configuration. The blue box represents the condition of having only 0 s inside that space time region.

where Π_L is a one-site shift operator for a chain of $2L$ sites with periodic boundaries. The local gate u implements the deterministic East model rule: a spin flips if its neighbor to the right—i.e., the one to the east—is in the state 1, or stays the same otherwise,

$$u = \begin{bmatrix} 1 & 0 & 0 & 0 \\ 0 & 0 & 0 & 1 \\ 0 & 0 & 1 & 0 \\ 0 & 1 & 0 & 0 \end{bmatrix}, \quad \langle n' m'|u|n\,m\rangle =: \;\; \begin{matrix} n' & & m' \\ & \square & \\ n & & m \end{matrix}$$

where our convention is $|0\rangle = [1\,0]^T$, $|1\rangle = [0\,1]^T$, and $|n\,m\rangle = |n\rangle \otimes |m\rangle$. The graphical representation of u allows to interpret the dynamics as a tensor network [46], see Fig. 1: panel (a) shows the allowed gates, while panel (b) gives the evolved state.

The Floquet-East model can also be thought of as a cellular automaton (CA), specifically rule 60 in the classification of Refs. [27,28]. In contrast to other recently studied CAs such as rule 54 [47–55], rule 201 [56,57], and rule 150 [58–60], rule 60 appears to be nonintegrable. Figure 1(c) shows a trajectory starting from a random initial configuration: the mixing nature of the dynamics is apparent, with fluctuations highly reminiscent of the dynamic heterogeneity and "space-time bubbles" of the stochastic (and continuous-time) East model [19]. This in turn suggests that much of the interesting behavior of stochastic KCMs might manifest in deterministic KCMs with the same constraints (see also [61,62]).

Propagation in space and invariant states. The definitions above describe the time evolution (down to up in Fig. 1) of configurations. Alternatively, one can consider also how a row pseudoprobability vector [63] $\langle \tilde{P}_x|$ over spins at a fixed point in space x and all times is propagated in space, $\langle \tilde{P}_{x+1}| = \langle \tilde{P}_x| \tilde{U}$ (from left to right in Fig. 1) under the dual operator $\tilde{U} = \tilde{U}^o \tilde{U}^e$, through the composition of the local gate

$$\tilde{u} := \begin{bmatrix} 1 & 0 & 0 & 0 \\ 0 & 0 & 0 & 1 \\ 0 & 0 & 0 & 1 \\ 1 & 0 & 0 & 0 \end{bmatrix}, \quad \langle n\,n'|\tilde{u}|m\,m'\rangle =: \;\; \begin{matrix} n' & & m' \\ & \square & \\ n & & m \end{matrix}, \quad (3)$$

and similarly defined evolution of a column vector $|\tilde{P}_x\rangle$ as $|\tilde{P}_{x-1}\rangle = \tilde{U}^o \tilde{U}^e |\tilde{P}_x\rangle$.

The time-dynamics is deterministic and reversible (i.e., a special case of bistochastic dynamics), which implies that the flat state is invariant under both the time evolution and its inverse. This is a local property of the gate u and can be stated graphically (see [45] for the details) as

$$\perp := \begin{bmatrix} 1 \\ 1 \end{bmatrix}, \quad \top := [1\ 1], \quad \square = \perp\perp, \quad \square = \top\top, \quad (4)$$

where, e.g., the last relation is $[1\ 1\ 1\ 1]u = [1\ 1\ 1\ 1]$. Similarly, the invariant states of the space dynamics [64] follow from a set of local algebraic relations satisfied by the local gates,

$$\vdash := [1\ 1], \quad \dashv := \begin{bmatrix} 1 \\ 1 \end{bmatrix}, \quad \subset := [1\ 0\ 0\ 1],$$

$$\square = 2\subset, \quad \square = \frac{\vdash}{\subset}, \quad \square = \frac{\subset}{\vdash}, \quad \square = \dashv. \quad (5)$$

From here we get that invariant states in space are, in the forward direction (left to right), the "dimerized state" obtained from the tensor product of $\subset$ (with appropriate boundaries, see below), and in the backward direction (right to left), the flat state. This is consistent with the space dynamics under $\tilde{U}$ being (right) stochastic, and is reminiscent of dual unitarity [65–67] (see also Refs. [68–81]) in the quantum setting.

Probability of inactive space-time regions. Relations Eqs. (4) and (5) allow to compute exactly several dynamical properties. Even though the dynamics is deterministic, if we consider a space-time region of size $l \times t$ inside a large box of $L \times T$, the dynamics in the region is probabilistic as the rest acts as an environment, and for $L, T \to \infty$ the circuit can be contracted to the boundary of the region in terms of the invariant states introduced above [82], see Fig. 2(a). As a first question, we consider the probability $P_{\text{inact}}(l, t)$ of having no spin flips in that space-time region. The probability $P_{\text{inact}}(l, t)$ is then obtained by contracting the region of inactive gates shown in Fig. 2(a), while the prefactor $2^{-(2l+\lfloor t \rfloor)}$ is determined as the factor needed to normalize to 1, the same region in the absence of conditioning. The inactive gates obey

$$\square = \supset \begin{smallmatrix} \phi \\ \phi \end{smallmatrix}, \quad \square = \supset \begin{smallmatrix} \phi \\ \phi \end{smallmatrix}, \quad (6)$$

with $\supset = \subset^T$ and ϕ denoting the projector onto the 0 state, $\phi = \begin{bmatrix} 1 & 0 \\ 0 & 0 \end{bmatrix}$. This means that the flat state on the right can be repeatedly propagated leftwards [see Fig. 2(a)], until we are left with

$$P_{\text{inact}}(l, t) = 2^{-(2l+\lfloor t \rfloor)} \times \perp = 2^{-(2l+\lfloor t \rfloor - 1)}. \quad (7)$$

The calculation is different for the special case of $t = 1/2$ (single row of inactive gates), as it reduces to the product of the expectation value of each gate [45]. Overall,

$$P_{\text{inact}}(l, t) = \begin{cases} 2^{-(2l+\lfloor t \rfloor - 1)}, & t \geqslant 1, \\ 2^{-l}, & t = \frac{1}{2}, \end{cases} \quad (8)$$

see Fig. 2(b). This is similar to the crossover observed numerically in the stochastic East model [10], and analogous to that in the free energy (i.e., minus log probability) of solvation
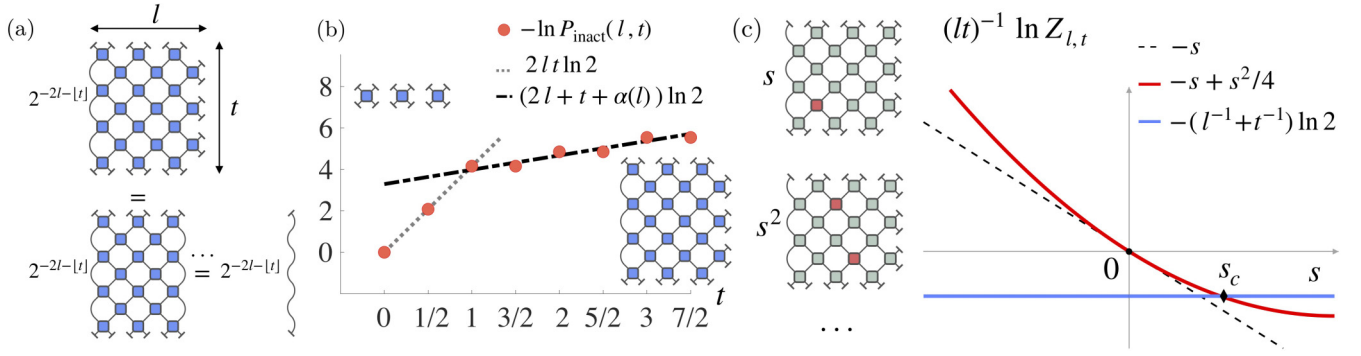
FIG. 2. Hydrophobic crossover and LD transition. (a) Graphical representation of $P_{\text{inact}}(l,t)$. The space-time region $l \times t$ is conditioned to only inactive gates (blue). This tensor network can be contracted to obtain Eq. (8). The prefactor $2^{-2l-\lfloor t\rfloor}$ ensures that in the absence of conditioning, the contraction is equal to one as required by probability conservation. (b) Corresponding dynamical free-energy $-\ln P_{\text{inact}}(l,t)$ as a function of time at $l = 3$, displaying a crossover from area (dotted gray line) to perimeter (dashed black line) scaling. The coefficient $\alpha(l)$ is $5/4$ for integer l. (c) The scaled CGF for the activity, $\ln Z_{l,t}(s)/lt$, has an active branch perturbatively connected to $s = 0$ (red), and an inactive branch coming from $s \to \infty$ (blue). Their crossing at $s_c \approx t^{-1} + l^{-1}$ indicates a first-order transition in trajectory space in the large l, t limit.

in the hydrophobic effect—from a regime dominated by entropy for small solutes, to one dominated by energy for large ones [7–9].

Phase transition in dynamical large deviations. The result above suggests that in the limit of $l, t \to \infty$ (with $l/L, t/T \to 0$) the Floquet-East model will have a phase transition in the space of trajectories [21,24,83]. This can be shown by considering the statistics of the dynamical activity (total number of spin flips) [21,23,84] in a space-time volume $l \times t$. Given the set of trajectories $\{\omega\}$ in the region, the moment generating function (MGF) of the activity is

$$Z_{l,t}(s) = \sum_{\omega} \pi(\omega)e^{-sK(\omega)}, \qquad (9)$$

where $\pi(\omega)$ is the probability of the trajectory and $K(\omega)$ its activity. The MGF is obtained from a calculation similar to that of Fig. 2(a), but where the active (spin-flip) gates carry an extra factor of e^{-s}.

Two limits are easy to calculate. In the limit of $s \to \infty$ all active gates are suppressed, and $Z_{l,t}(s)$ is given by Eq. (8). Conversely, for $s \approx 0$ we can express $Z_{l,t}(s)$ as a series in s with the moments of the activity as coefficients,

$$Z_{l,t}(s) = 1 - s\langle K\rangle + \tfrac{1}{2}s^2\langle K^2\rangle + \cdots . \qquad (10)$$

The first two moments are obtained straightforwardly,

$$\langle K\rangle = lt, \quad \langle K^2\rangle = (lt)^2/2, \qquad (11)$$

the latter result given by the fact that all two-point correlators are disconnected in the dynamics [45]. The difference in scaling for small and large s implies a crossover in the cumulant generating function (CGF), $\ln Z_{l,t}(s)$, which, in the limit of $l, t \to \infty$, becomes singular, see Fig. 2(c). Since the CGF is convex and nonincreasing [24], the perturbative branch (red curve) has to cross to the inactive branch (blue curve), with the change becoming progressively sharp and occurring around $s_c \approx 1/l + 1/t$. For $l, t \to \infty$ this corresponds to a discontinuity in the derivative of the CGF at $s = 0$, and therefore the model has to undergo an active-inactive first-order phase transition. This transition (cf. liquid-vapor in water) gives rise to the dynamic hydrophobicity in the model.

Solvation in space time. To draw an analogy with the case of a solute in water, we consider the probability of a region of space time with all sites in the zero state. See Fig. 3(a) for the tensor network representation; given a region $l \times t$ with all spins conditioned to be in the 0 state, we can compute the probability of this event, $P_{\square}(l,t)$, as before, by contracting the outside to the edges of the region using the invariant states. Noting that

and using the relations (6) for the inactive gates, we get that for integer t the probability is $\frac{1}{2}$ of the corresponding region being inactive, [85]

$$P_{\square}(l,t) = 2^{-(2l+\lfloor t-\frac{1}{2}\rfloor)}. \qquad (13)$$

The key observation is that the free-energy cost for a fluctuation as that of Fig. 3(a) scales with the perimeter, $2l + t$, of the region, rather than with the total number of sites in the region, $4lt$. This calculation can be repeated for other shapes of the conditioned region. It is easy to show that the optimal one is that of an isosceles right-pointing triangle, see Fig. 3(b): the probability in this case goes as [45]

$$P_{\triangleright}(t) = 2^{-t}. \qquad (14)$$

For comparison, a rectangle with the same number of conditioned 0 sites would have a smaller probability of occurring, $P_{\square}(t + 1, t/2) \propto 2^{-3t/2}$ [86].

The optimality of the right-pointing triangle is shown by computing the average spin density, $\rho(\Delta x, \Delta t)$, at a distance $(\Delta x, \Delta t)$ from a region conditioned to have all 0 spins: see Figs. 3(c) and 3(d), where $\blacklozenge = \begin{bmatrix} 0 & 0 \\ 0 & 1 \end{bmatrix}$ projects to the state 1. When the location of the projector is near the solute, as in panel (c), all sites within the enclosing triangle (shaded region) are also 0 at no extra free-energy cost; for the probed site to be 1 would require a nonexistent gate (circled), cf. Fig. 1(a), and as a consequence, $\rho(\Delta x, \Delta t) = 0$ for any site within the shaded triangle [45]. In contrast, for sites outside the triangle, the contraction decouples the site, Fig. 3(d),
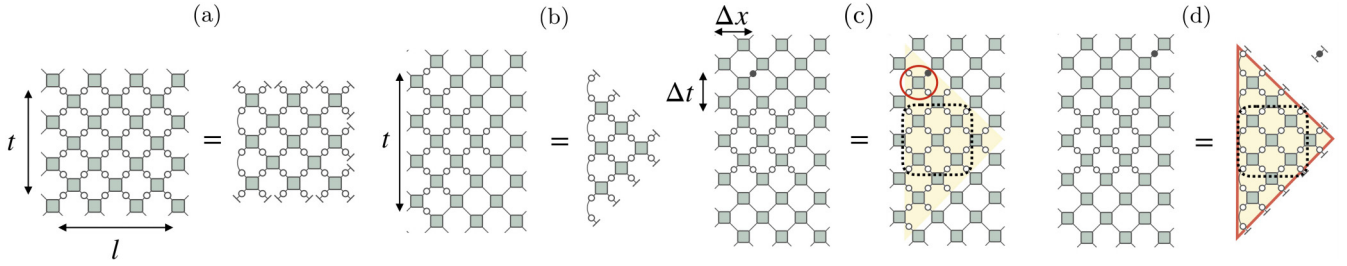
FIG. 3. Solvation and optimal void geometry. (a) Network representation of the probability $P_\square(l, t)$ of a square region conditioned to all zero spins, embedded in a much larger trajectory. (b) Same for $P_\triangleright(t)$ for the optimal triangular geometry. (c) Spin density outside from the condition: when the site falls inside the triangle (shaded area) enclosing the condition (dashed square) the density is zero (due to the impossible gate, circled in red). (d) Same but now the probed site falls outside the enclosing triangle; in this case the density is the average one.

which gives the stationary-state value, $\rho(\Delta x, \Delta t) = 1/2$. The above reasoning shows that to accommodate any space-time "solute," the most efficient fluctuation is to create a triangular "bubble," which encloses the solute by locally phase separating the dynamics. The optimal shape also explains the nature of the dynamical fluctuations observed in trajectories such as that of Fig. 1(c) where the bubbles are all right-pointing triangles.

Hydrophobic collapse. The free energy of a single solute scaling with the interface of the enclosing bubble leads to an interaction when two or more solutes are present. In water this is known as hydrophobic collapse [87]. In the dynamics of the Floquet-East model we have the same in space time: Fig. 4(a) shows two space-time regions (light blue rectangles) conditioned to having all their spins in the zero state, with the two regions separated in space by a distance Δx. For large Δx

FIG. 4. Hydrophobic collapse. (a) Two space-time "solutes" (light blue) of size $l \times t$ separated in space by Δx. Conditions on empty boxes extend to triangular shaped regions (dark blue and yellow). (b) Dynamical free energy as a function of Δx. This is given by the perimeter of the optimal triangular bubble enclosing the two boxes (orange contour): for large Δx it is given by the perimeters of two triangles enclosing each condition individually, as the probabilities factorize for $\Delta x \geqslant t/2$; for $\Delta x < t/2$, the free energy is given by the perimeter of a single larger bubble enclosing both conditions, and decreases with decreasing distance giving rise to an effective attraction. The coefficients are $a(l, t) = \ln 2(4l + t - 1/2)$, $c = \ln 2/2$. (c), (d) Same for a time separation of Δt. The coefficients in (d) are $b(l, t) = \ln 2(2l + 2t - 3/4)$, $c = \ln 2/2$.

each of these conditions gives rise to a triangular bubble that encloses it, and the (dynamical) free-energy cost is given by the sum of the perimeters of the two triangles. However, as Δx decreases, we eventually reach a point beyond which it is more favorable to enclose both solutes within a single triangular bubble, and as Δx is reduced further the free energy also goes down, see Fig. 4(b). This gives rise to the "attraction" between the solutes, a dynamical version of hydrophobic collapse. Figures 4(c) and 4(d) show the same for separation in the time direction.

Pretransition effects in the stochastic model. The stochastic version of the Floquet East model is defined by the following six possible gates [44]:

$$
\begin{matrix} n_1' & & n_2' \\ & \boxed{\mathbf{P}} & \\ n_1 & & n_2 \end{matrix} = \left[\delta_{n_2,0}\delta_{n_1',n_1} + \delta_{n_2,1}\left(p\,\delta_{n_1',1-n_1} + \bar{p}\,\delta_{n_1',n_1}\right) \right] \delta_{n_2',n_2}.
$$

Here the constraint is the same as before, but if a flip is possible it only occurs with probability p (with no change with probability $\bar{p} = 1 - p$). The deterministic model is recovered for $p = 1$. The stochastic circuit and the standard (continuous-time) stochastic East model [15] are directly connected through the Trotter-Suzuki decomposition of the integrated time-evolution operator [88,89].

As proved in Ref. [44], the results for the deterministic model ($p = 1$) imply similar dynamic hydrophobicity for the stochastic ($p < 1$) case. Specifically, one can show that the probability of an inactive space-time region is bounded from below by the deterministic result [44]

$$
P_{\text{inact}}^{(p)}(l, t) \geqslant P_{\text{inact}}^{(p=1)}(l, t) = 2^{-(2l+\lfloor t \rfloor - 1)} \quad (t \geqslant 1).
$$

Similar lower bounds are found for the probabilities of regions of all 0 spins, cf. Eqs. (13) and (14) [44]. This demonstrates [44] that the stochastic Floquet-East has an active/inactive first-order transition, and the space-time perimeter scaling of the dynamical-free energy of inactive regions is analogous to the area (rather than volume) dependence of the free energy for cavities in water [7,8].

Conclusions. Here we studied the Floquet-East model, a circuit version of the kinetically constrained East model. We proved analytically that its trajectories display pretransition effects, a dynamical analog of the hydrophobic effect in water. We computed the exact probabilities for inactive space-time fluctuations for the deterministic limit of the model.
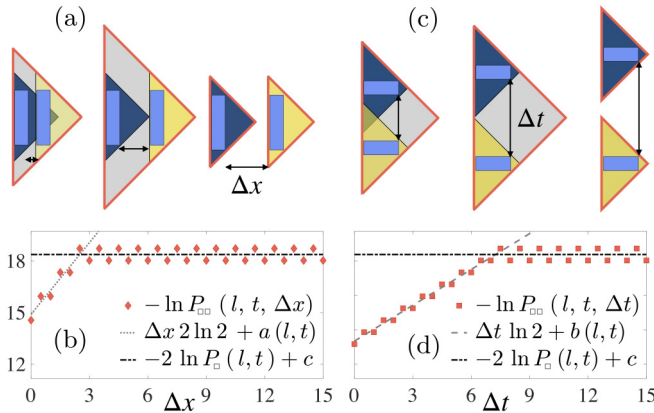
Moreover, as we prove in Ref. [44], the results for the deterministic circuit lower-bound probability of inactive fluctuations in the stochastic version of the model. The work here is classical, but since the deterministic Floquet-East is also unitary, our results connect to the ongoing interest in the dynamics of quantum circuits, e.g., [65,69,73,90–100]. For example, one could consider (with small alterations, cf. [101–103]) quantum dynamics, where we expect similar hydrophobic fluctuations to play an important role in entanglement growth and thermalization [36,104].

[1] H. B. Casimir, Proc. Kon. Ned. Akad. Wet. **51**, 793 (1948).

[2] M. E. Fisher and P. G. Gennes, C. R. Acad. Sci. Paris **287**, 207 (1978).

[3] C. Hertlein, L. Helden, A. Gambassi, S. Dietrich, and C. Bechinger, Nature (London) **451**, 172 (2008).

[4] A. Gambassi, J. Phys. **161**, 012037 (2009).

[5] R. Lipowsky, Phys. Rev. Lett. **49**, 1575 (1982).

[6] R. Lipowsky, J. Appl. Phys. **55**, 2485 (1984).

[7] K. Lum, D. Chandler, and J. D. Weeks, J. Phys. Chem. B **103**, 4570 (1999).

[8] D. Chandler, Nature (London) **437**, 640 (2005).

[9] S. Katira, K. K. Mandadapu, S. Vaikuntanathan, B. Smit, and D. Chandler, Elife **5**, e13150 (2016).

[10] S. Katira, J. P. Garrahan, and K. K. Mandadapu, Phys. Rev. Lett. **120**, 260602 (2018).

[11] G. H. Fredrickson and H. C. Andersen, Phys. Rev. Lett. **53**, 1244 (1984).

[12] J. Jöckle and S. Eisinger, Z. Phys. B **84**, 115 (1991).

[13] F. Ritort and P. Sollich, Adv. Phys. **52**, 219 (2003).

[14] D. Chandler and J. P. Garrahan, Annu. Rev. Phys. Chem. **61**, 191 (2010).

[15] J. P. Garrahan, Physica A **504**, 130 (2018).

[16] T. Speck, J. Stat. Mech. (2019) 084015.

[17] L. Berthier and G. Biroli, Rev. Mod. Phys. **83**, 587 (2011).

[18] G. Biroli and J. P. Garrahan, J. Chem. Phys. **138**, 12A301 (2013).

[19] J. P. Garrahan and D. Chandler, Phys. Rev. Lett. **89**, 035704 (2002).

[20] M. Merolle, J. P. Garrahan, and D. Chandler, Proc. Natl. Acad. Sci. USA **102**, 10837 (2005).

[21] J. P. Garrahan, R. L. Jack, V. Lecomte, E. Pitard, K. van Duijvendijk, and F. van Wijland, Phys. Rev. Lett. **98**, 195702 (2007).

[22] J. P. Garrahan, R. L. Jack, V. Lecomte, E. Pitard, K. van Duijvendijk, and F. van Wijland, J. Phys. A **42**, 075007 (2009).

[23] V. Lecomte, C. Appert-Rolland, and F. van Wijland, J. Stat. Phys. **127**, 51 (2007).

[24] H. Touchette, Phys. Rep. **478**, 1 (2009).

[25] R. L. Jack, Eur. Phys. J. B **93**, 74 (2020).

[26] M. Esposito, U. Harbola, and S. Mukamel, Rev. Mod. Phys. **81**, 1665 (2009).

[27] S. Wolfram, Rev. Mod. Phys. **55**, 601 (1983).

[28] A. Bobenko, M. Bordemann, C. Gunn, and U. Pinkall, Commun. Math. Phys. **158**, 127 (1993).

[29] B. Buča, K. Klobas, and T. Prosen, J. Stat. Mech. (2021) 074001.

[30] I. Lesanovsky, Phys. Rev. Lett. **106**, 025301 (2011).

[31] I. Lesanovsky and J. P. Garrahan, Phys. Rev. Lett. **111**, 215305 (2013).

[32] V. D. Naik, F. B. Trigueros, and M. Heyl, arXiv:2311.16240.

[33] T. Zhang and Z. Cai, Phys. Rev. Lett. **132**, 206503 (2024).

[34] M. van Horssen, E. Levi, and J. P. Garrahan, Phys. Rev. B **92**, 100305(R) (2015).

[35] A. Smith, J. Knolle, D. L. Kovrizhin, and R. Moessner, Phys. Rev. Lett. **118**, 266601 (2017).

[36] Z. Lan, M. van Horssen, S. Powell, and J. P. Garrahan, Phys. Rev. Lett. **121**, 040603 (2018).

[37] N. Pancotti, G. Giudice, J. I. Cirac, J. P. Garrahan, and M. C. Bañuls, Phys. Rev. X **10**, 021051 (2020).

[38] S. Roy and A. Lazarides, Phys. Rev. Res. **2**, 023159 (2020).

[39] R. J. Valencia-Tortora, N. Pancotti, and J. Marino, PRX Quantum **3**, 020346 (2022).

[40] C. J. Turner, A. A. Michailidis, D. A. Abanin, M. Serbyn, and Z. Papić, Nat. Phys. **14**, 745 (2018).

[41] S. Moudgalya, B. A. Bernevig, and N. Regnault, Rep. Prog. Phys. **85**, 086501 (2022).

[42] R. M. Nandkishore and M. Hermele, Annu. Rev. Condens. Matter Phys. **10**, 295 (2019).

[43] M. Pretko, X. Chen, and Y. You, Int. J. Mod. Phys. A **35**, 2030003 (2020).

[44] C. D. Fazio, J. P. Garrahan, and K. Klobas, arXiv:2406.17464.

[45] See Supplemental Material at http://link.aps.org/supplemental/10.1103/PhysRevE.110.L022101 for a graphical summary of the properties of the local gates, the additional details on the hydrophobic crossover, dynamical large deviations, hydrophobic collapse, and a characterization of an inhomogeneous quench.

[46] Tensor Network https://tensornetwork.org, Accessed: 21-12-2023.

[47] T. Prosen and C. Mejía-Monasterio, J. Phys. A: Math. Theor. **49**, 185003 (2016).

[48] A. Inoue and S. Takesue, J. Phys. A: Math. Theor. **51**, 425001 (2018).

[49] T. Prosen and B. Buča, J. Phys. A: Math. Theor. **50**, 395002 (2017).

[50] S. Gopalakrishnan, Phys. Rev. B **98**, 060302(R) (2018).

[51] B. Buča, J. P. Garrahan, T. Prosen, and M. Vanicat, Phys. Rev. E **100**, 020103(R) (2019).

[52] K. Klobas and T. Prosen, SciPost Phys. Core **2**, 010 (2020).

[53] K. Klobas, M. Medenjak, T. Prosen, and M. Vanicat, Commun. Math. Phys. **371**, 651 (2019).

[54] V. Alba, J. Dubail, and M. Medenjak, Phys. Rev. Lett. **122**, 250603 (2019).

[55] K. Klobas, M. Vanicat, J. P. Garrahan, and T. Prosen, J. Phys. A: Math. Theor. **53**, 335001 (2020).

[56] J. W. P. Wilkinson, K. Klobas, T. Prosen, and J. P. Garrahan, Phys. Rev. E **102**, 062107 (2020).

[57] T. Iadecola and S. Vijay, Phys. Rev. B **102**, 180302(R) (2020).

[58] S. Gopalakrishnan and B. Zakirov, Quantum Sci. Technol. **3**, 044004 (2018).

[59] T. Gombor and B. Pozsgay, Phys. Rev. E **104**, 054123 (2021).

[60] J. W. P. Wilkinson, T. Prosen, and J. P. Garrahan, Phys. Rev. E **105**, 034124 (2022).

[61] A. Deger, S. Roy, and A. Lazarides, Phys. Rev. Lett. **129**, 160601 (2022).

[62] A. Deger, A. Lazarides, and S. Roy, Phys. Rev. Lett. **129**, 190601 (2022).

[63] Note that the vector $\langle \tilde{P}_x |$ is not necessarily a valid probability vector since it does not need to be normalized.

[64] In the quantum setup, analogous objects—the left and right fixed points of the space transfer matrix—are referred to also as influence matrices [82]. These have recently been understood to provide convenient numerical [82,105–109] and analytical tools [65,69,72,80,101–103,110–112] to study quantum many-body dynamics.

[65] B. Bertini, P. Kos, and T. Prosen, Phys. Rev. Lett. **123**, 210601 (2019).

[66] P. Kos, B. Bertini, and T. Prosen, Phys. Rev. X **11**, 011022 (2021).

[67] P. Kos and G. Styliaris, Quantum **7**, 1020 (2023).

[68] B. Bertini, P. Kos, and T. Prosen, Phys. Rev. Lett. **121**, 264101 (2018).

[69] B. Bertini, P. Kos, and T. Prosen, Phys. Rev. X **9**, 021033 (2019).

[70] B. Bertini, P. Kos, and T. Prosen, SciPost Phys. **8**, 067 (2020).

[71] B. Bertini, P. Kos, and T. Prosen, SciPost Phys. **8**, 068 (2020).

[72] L. Piroli, B. Bertini, J. I. Cirac, and T. Prosen, Phys. Rev. B **101**, 094304 (2020).

[73] P. W. Claeys and A. Lamacraft, Phys. Rev. Res. **2**, 033032 (2020).

[74] P. W. Claeys and A. Lamacraft, Phys. Rev. Lett. **126**, 100603 (2021).

[75] B. Bertini, P. Kos, and T. Prosen, Commun. Math. Phys. **387**, 597 (2021).

[76] C. Jonay, V. Khemani, and M. Ippoliti, Phys. Rev. Res. **3**, 043046 (2021).

[77] Y. Kasim and T. Prosen, J. Phys. A: Math. Theor. **56**, 025003 (2023).

[78] R. Suzuki, K. Mitarai, and K. Fujii, Quantum **6**, 631 (2022).

[79] A. Foligno and B. Bertini, Phys. Rev. B **107**, 174311 (2023).

[80] A. Foligno, T. Zhou, and B. Bertini, Phys. Rev. X **13**, 041008 (2023).

[81] M. A. Rampp, R. Moessner, and P. W. Claeys, Phys. Rev. Lett. **130**, 130402 (2023).

[82] A. Lerose, M. Sonner, and D. A. Abanin, Phys. Rev. X **11**, 021040 (2021).

[83] R. L. Jack, T. Nemoto, and V. Lecomte, J. Stat. Mech. (2020) 053204.

[84] C. Maes, Phys. Rep. **850**, 1 (2020).

[85] Note that $P_\square(l, t)$ scales with $P_{\text{inact}}(l - \frac{1}{2}, t - \frac{1}{2})$ due to the way that the sizes are defined in both cases: in the former

the size corresponds to the number of unit cells (i.e., twice the number of sites), while in the latter the number of time/space steps. This subtlety arises because of the way that the constraints are applied—either to sites or gates. See [45] for an illustration.

[86] In the deterministic model, similar perimeter scaling is obtained for the free energies of space-time regions corresponding to allowed trajectories of the circuit. In contrast, only regions of 0 s show this scaling in the stochastic case. See [45] for details.

[87] A. P. Willard and D. Chandler, J. Phys. Chem. B **112**, 6187 (2008).

[88] H. F. Trotter, Proc. Am. Math. Soc. **10**, 545 (1959).

[89] M. Suzuki, J. Math. Phys. **32**, 400 (1991).

[90] T. J. Osborne, Phys. Rev. Lett. **97**, 157202 (2006).

[91] A. Nahum, J. Ruhman, S. Vijay, and J. Haah, Phys. Rev. X **7**, 031016 (2017).

[92] A. Nahum, S. Vijay, and J. Haah, Phys. Rev. X **8**, 021014 (2018).

[93] A. Chan, A. De Luca, and J. T. Chalker, Phys. Rev. X **8**, 041019 (2018).

[94] C. W. von Keyserlingk, T. Rakovszky, F. Pollmann, and S. L. Sondhi, Phys. Rev. X **8**, 021013 (2018).

[95] S. Gopalakrishnan and A. Lamacraft, Phys. Rev. B **100**, 064309 (2019).

[96] A. J. Friedman, A. Chan, A. De Luca, and J. T. Chalker, Phys. Rev. Lett. **123**, 210603 (2019).

[97] Y. Li, X. Chen, and M. P. A. Fisher, Phys. Rev. B **100**, 134306 (2019).

[98] B. Skinner, J. Ruhman, and A. Nahum, Phys. Rev. X **9**, 031009 (2019).

[99] T. Rakovszky, F. Pollmann, and C. W. von Keyserlingk, Phys. Rev. Lett. **122**, 250602 (2019).

[100] A. Zabalo, M. J. Gullans, J. H. Wilson, S. Gopalakrishnan, D. A. Huse, and J. H. Pixley, Phys. Rev. B **101**, 060301(R) (2020).

[101] K. Klobas, B. Bertini, and L. Piroli, Phys. Rev. Lett. **126**, 160602 (2021).

[102] K. Klobas and B. Bertini, SciPost Phys. **11**, 106 (2021).

[103] K. Klobas and B. Bertini, SciPost Phys. **11**, 107 (2021).

[104] B. Bertini, C. De Fazio, J. P. Garrahan, and K. Klobas, Phys. Rev. Lett. **132**, 120402 (2024).

[105] M. C. Bañuls, M. B. Hastings, F. Verstraete, and J. I. Cirac, Phys. Rev. Lett. **102**, 240603 (2009).

[106] A. Müller-Hermes, J. I. Cirac, and M. C. Bañuls, New J. Phys. **14**, 075003 (2012).

[107] M. Sonner, A. Lerose, and D. A. Abanin, Ann. Phys. **435**, 168677 (2021).

[108] A. Lerose, M. Sonner, and D. A. Abanin, Phys. Rev. B **104**, 035137 (2021).

[109] M. Frías-Pérez and M. C. Bañuls, Phys. Rev. B **106**, 115117 (2022).

[110] G. Giudice, G. Giudici, M. Sonner, J. Thoenniss, A. Lerose, D. A. Abanin, and L. Piroli, Phys. Rev. Lett. **128**, 220401 (2022).

[111] B. Bertini, K. Klobas, and T.-C. Lu, Phys. Rev. Lett. **129**, 140503 (2022).

[112] B. Bertini, K. Klobas, V. Alba, G. Lagnese, and P. Calabrese, Phys. Rev. X **12**, 031016 (2022).